2013

# Contributions of VLDLR and LRP8 in the establishment of retinogeniculate projections

Jianmin Su
*Virginia Polytechnic Institute and State University*

Michael A. Klemm
*Virginia Polytechnic Institute and State University*

Anne M. Josephson
*Virginia Commonwealth University*

Michael A. Fox
*Virginia Commonwealth University*

Neural Development

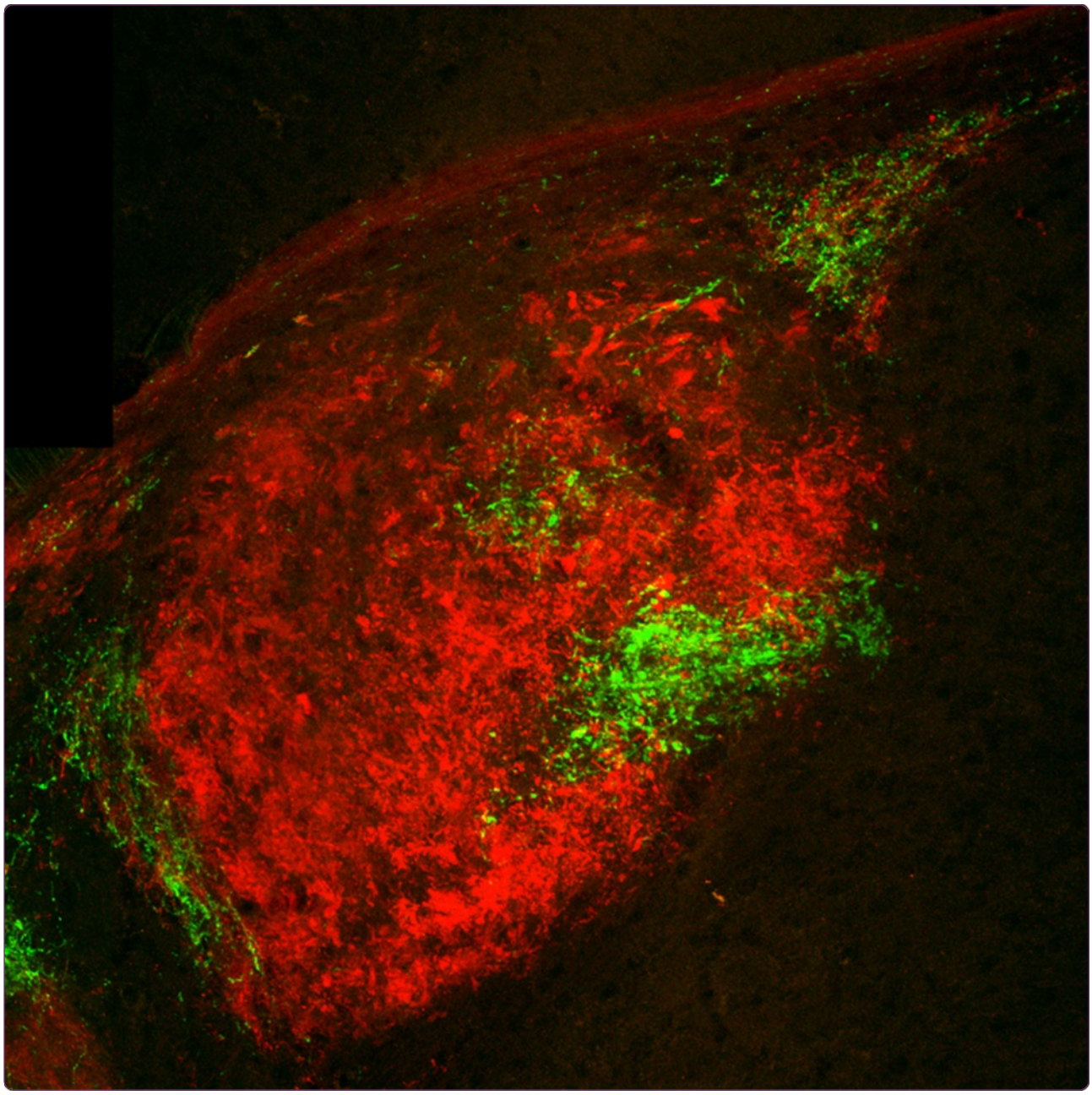

# Contributions of VLDLR and LRP8 in the establishment of retinogeniculate projections

Su *et al.*

BioMed Central

Su *et al. Neural Development* 2013, **8**:11
http://www.neuraldevelopment.com/content/8/1/11

Su et al. Neural Development 2013, 8:11
http://www.neuraldevelopment.com/content/8/1/11

Neural Development

RESEARCH ARTICLE Open Access

# Contributions of VLDLR and LRP8 in the establishment of retinogeniculate projections

Jianmin Su[1], Michael A Klemm[2], Anne M Josephson[3] and Michael A Fox[1,2,3*]

## Abstract

**Background:** Retinal ganglion cells (RGCs), the output neurons of the retina, project to over 20 distinct brain nuclei, including the lateral geniculate nucleus (LGN), a thalamic region comprised of three functionally distinct subnuclei: the ventral LGN (vLGN), the dorsal LGN (dLGN) and the intergeniculate leaflet (IGL). We previously identified reelin, an extracellular glycoprotein, as a critical factor that directs class-specific targeting of these subnuclei. Reelin is known to bind to two receptors: very-low-density lipoprotein receptor (VLDLR) and low-density lipoprotein receptor-related protein 8 (LRP8), also known as apolipoprotein E receptor 2 (ApoER2). Here we examined the roles of these canonical reelin receptors in retinogeniculate targeting.

**Results:** To assess the roles of VLDLR and LRP8 in retinogeniculate targeting, we used intraocular injections of fluorescently conjugated cholera toxin B subunit (CTB) to label all RGC axons *in vivo*. Retinogeniculate projections in mutant mice lacking either VLDLR or LRP8 appeared similar to controls; however, deletion of both receptors resulted in dramatic defects in the pattern of retinal innervation in LGN. Surprisingly, defects in *vldlr*$^{-/-}$;*lrp8*$^{-/-}$ double mutant mice were remarkably different than those observed in mice lacking reelin. First, we failed to observe retinal axons exiting the medial border of the vLGN and IGL to invade distant regions of non-retino-recipient thalamus. Second, an ectopic region of binocular innervation emerged in the dorsomedial pole of *vldlr*$^{-/-}$;*lrp8*$^{-/-}$ mutant dLGN. Analysis of retinal projection development, retinal terminal sizes and LGN cytoarchitecture in *vldlr*$^{-/-}$;*lrp8*$^{-/-}$ mutants, all suggest that a subset of retinal axons destined for the IGL are misrouted to the dorsomedial pole of dLGN in the absence of VLDLR and LRP8. Such mistargeting is likely the result of abnormal migration of IGL neurons into the dorsomedial pole of dLGN in *vldlr*$^{-/-}$;*lrp8*$^{-/-}$ mutants.

**Conclusions:** In contrast to our expectations, the development of both the LGN and retinogeniculate projections appeared dramatically different in mutants lacking either reelin or both canonical reelin receptors. These results suggest that there are reelin-independent functions of VLDLR and LRP8 in LGN development, and VLDLR- and LRP8-independent functions of reelin in class-specific axonal targeting.

**Keywords:** Reelin, Synaptic targeting, Intergeniculate nucleus, Retinogeniculate, Lateral geniculate nucleus, Axon, Retinal terminal

## Background

Neural circuits associated with retinal ganglion cells (RGCs) have long been used as models for investigating the mechanisms that underlie circuit development and function. As the sole output neurons of the retina, RGCs must convey information regarding color, contrast, light intensity and object movement to specific regions within retino-recipient nuclei of the brain. For this reason, RGC axons project to over 20 distinct central nervous system (CNS) nuclei and are targeted to these sites by at least three distinct mechanisms. First, retinal axons are sorted topographically, so that the location of information in the visual field is accurately conveyed to a spatially correlated region of a retino-recipient nucleus [1]. Ephs/ephrins, morphogens and transmembrane cell adhesion molecules all contribute to topographic targeting of retinal axons in the mammalian brain [1-3]. In addition to being topographically mapped, retinal axons are sorted into discrete domains of most retino-recipient nuclei based upon their eye of origin. The formation of eye-specific domains requires both

* Correspondence: mafox1@vtc.vt.edu
[1]Virginia Tech Carilion Research Institute, Roanoke, VA 24016, USA
[2]Department of Biological Sciences, Virginia Tech, Blacksburg, VA 24061, USA
Full list of author information is available at the end of the article

axonal targeting cues (such as Eph/ephrins and teneurins) [4-6], and subsequent activity-dependent refining signals (such as MHC1, C1q and neuronal pentraxins) [7-10]. The third targeting mechanism involves axons from different functional classes of RGCs targeting distinct retino-recipient nuclei or different lamina (or domains) with these nuclei. Although axonal projection patterns have recently been described for several classes of RGCs [11-19], few studies have shed light on the mechanisms underlying such class-specific targeting [20]. We recently identified reelin as a critical regulator of class-specific retinogeniculate targeting.

Reelin is a bulky, extracellular glycoprotein composed of an N-terminal f-spondin domain, eight repeated unique domains containing epidermal growth factor (EGF)-like motifs and a C-terminal domain rich in positively charged amino acids [21,22]. A multitude of studies have shown roles for reelin in neuronal migration, axonal polarization, dendritic arborization and spine formation, growth cone guidance, axonal targeting, and synaptic function and plasticity [21-30]. We previously identified reelin in a screen for synaptic targeting cues that were differentially expressed in subnuclei of the lateral geniculate nucleus (LGN): the ventral LGN (vLGN), the dorsal LGN (dLGN) and the intergeniculate leaflet (IGL) [31]. Reelin is significantly enriched in vLGN and IGL during retinogeniculate circuit formation, and mice lacking reelin ($reln^{rl/rl}$) exhibit severe defects in retinal targeting of these regions [31]. Targeting defects in $reln^{rl/rl}$ mutants result from the mistargeting of intrinsically photosensitive RGC (ipRGC) axons, whereas axons from other classes of RGCs appear unaffected by the absence of reelin [31].

Most functions of reelin have been attributed to its ability to bind two members of the low- density lipoprotein (LDL) receptor gene family: very-low-density lipoprotein receptor (VLDLR) and low-density lipoprotein receptor-related protein 8 (LRP8), also known as apolipoprotein E receptor 2 (ApoER2) [32,33]. Upon binding reelin, VLDLR and LRP8 activate the intracellular adaptor molecule disabled-1 (DAB1) [32]. Genetic deletion of both VLDLR and LRP8 or DAB1 result in mutant mice that outwardly resemble $reln^{rl/rl}$ mutants [32,34-36]. Our previous studies on visual system development partially confirmed a similar molecular signaling pathway underlies reelin's function in retinal targeting: mice harboring a spontaneous mutation in DAB1 exhibit similar defects in retinogeniculate targeting as $reln^{rl/rl}$ mutants [31]. In the present study we sought to expand these findings and test the roles of VLDLR and LRP8 in retinogeniculate targeting. We hypothesized that deletion of both canonical reelin receptors would produce defects in retinal targeting that closely resembled those in the absence of reelin. To our surprise, however, defects observed in mice lacking both VLDLR and LRP8 ($vldlr^{-/-}$;$lrp8^{-/-}$) were strikingly different than those in reeler mutants. Results presented here suggest that there are both reelin-independent functions of VLDLR and LRP8, and VLDLR- and LRP8-independent functions of reelin in visual system development.

## Results

### Deletion of both VLDLR and LRP8 disrupts retinogeniculate targeting

To assess the roles of VLDLR and LRP8 in retinogeniculate targeting we analyzed retinal projections in $vldlr^{-/-}$ and $lrp8^{-/-}$ mutant mice. These mice are viable, fertile, and their appearance and cage behavior are indistinguishable from wild-type and heterozygote littermates. Intraocular injections of fluorescently conjugated cholera toxin B subunit (CTB) were used to label all RGC axons. Axonal projections were analyzed during the second and third postnatal weeks of mouse development, a period of development when retinal axons have fully innervated the dLGN, vLGN and IGL (Figure 1A). Projections from each eye were labeled with distinct fluorescently conjugated versions of CTB, so that eye-specific projections could be distinguished in the LGN. In contrast to mutants lacking reelin (Figure 1B), the gross pattern of retinal projections to each LGN subnuclei in mutants lacking either VLDLR or LRP8 appeared similar to those observed in littermate controls in many regards (Figure 1C,D). Specifically, retinal axons fully arborized in the IGL, and no retinal axons were observed exiting the medial border of the vLGN or IGL and invading non-retino-recipient regions of medial thalamus (Figure 1C,D and see arrowheads in 1B) (Table 1). Although these gross patterns of retinal innervation in $vldlr^{-/-}$ and $lrp8^{-/-}$ mutant mice appeared similar to littermate controls, the absence of these receptors (and reelin) clearly affected activity-dependent refinement of retinal projections into fully segregated, eye-specific domains in both vLGN and dLGN.

Previous studies have demonstrated that VLDLR and LRP8 are capable of compensating for each other [32]. For this reason, we explored whether deletion of both VLDLR and LRP8 affects retinogeniculate targeting. $Vldlr^{-/-}$;$lrp8^{-/-}$ double mutant mice are born in expected ratios and are indistinguishable from littermate controls (or $vldlr^{-/-}$ or $lrp8^{-/-}$ single mutants) at birth. By the end of the first week of postnatal development, $vldlr^{-/-}$; $lrp8^{-/-}$ mutants appeared smaller than littermates and by postnatal day 12 (P12) double mutants exhibited an ataxic gait (similar to $reln^{rl/rl}$ mutants). Retinal projections were labeled by intraocular injection of CTB in P9 to P23 $vldlr^{-/-}$;$lrp8^{-/-}$ mutants (n = 6). Several defects in retinal projections in the absence of both VLDLR and LRP8 appeared similar to defects observed in mutants lacking reelin (Figure 1B and 2B,C). Specifically, the spatial extent of retinal innervation to vLGN and IGL appeared markedly decreased in $vldlr^{-/-}$;$lrp8^{-/-}$ mutants

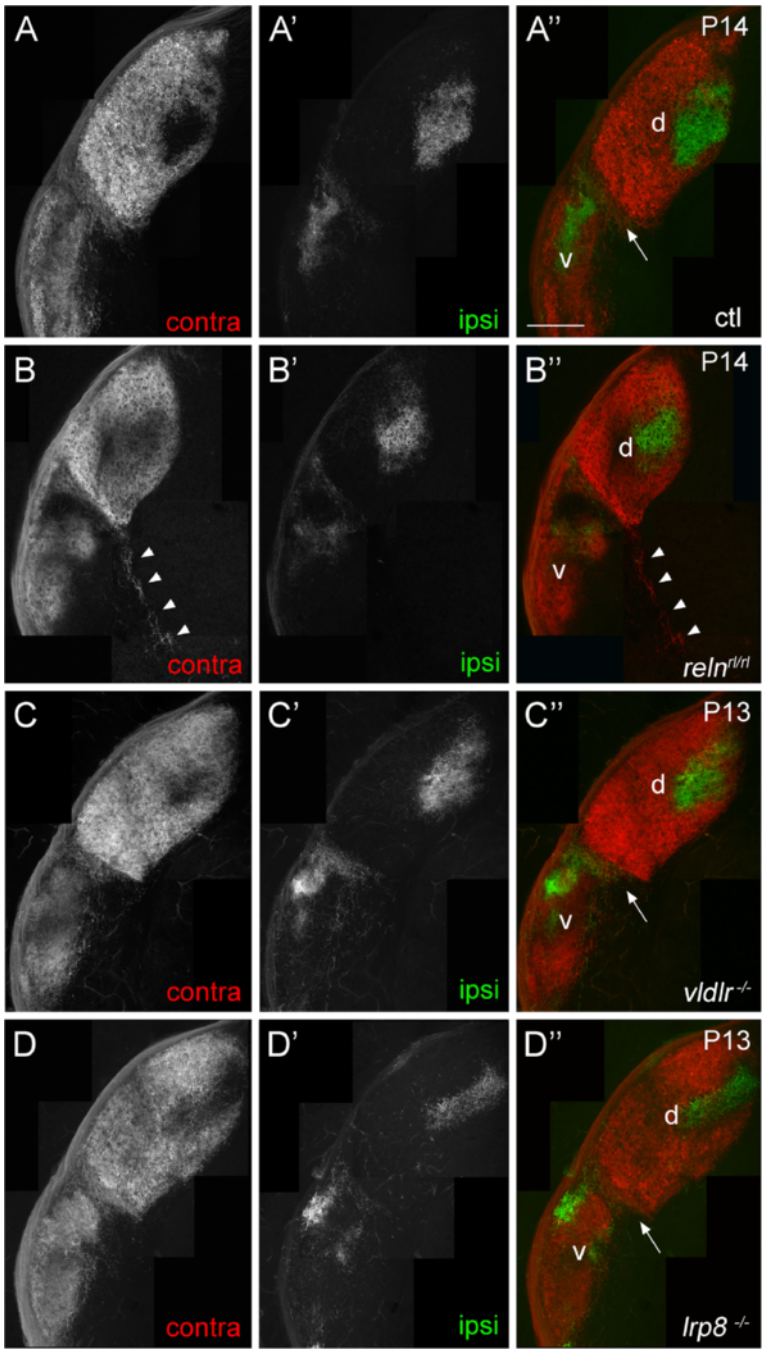


**Figure 1 Retinogeniculate projections in wild-type, *reln*$^{rl/rl}$, *vldlr*$^{-/-}$ and *lrp8*$^{-/-}$mice.** Retinogeniculate projections in **(A)** P14 controls, **(B)** P14 *reln*$^{rl/rl}$ mutants, **(C)** P13 *vldlr*$^{-/-}$ mutants and **(D)** P13 *lrp8*$^{-/-}$ mutants were labeled by intraocular injection of fluorescently conjugated CTB. Left eyes were injected with Alexa Fluor 594 CTB and right eyes were injected with Alexa Fluor 488 CTB. LGN from right hemispheres are shown. In P14 *reln*$^{rl/rl}$ mutants (**B**), note the near absence of retinal projections to the IGL, and the bundle of labeled retinal axons extending out of the LGN and into non-retino-recipient thalamus (arrowheads). 'Contra' denotes projections originating from the contralateral retina and 'ipsi' denotes projections originating from the ipsilateral retina. dLGN are labeled 'd', vLGN are labeled 'v' and arrows indicate IGL. The color of the label in panels (**A** to **D**) and (**A'** to **D'**) indicates the color of the image shown in (**A''** to **D''**). Scale bar = 200 μm. CTB, cholera toxin B subunit; dLGN, dorsal LGN; IGL, intergeniculate leaflet; LGN, lateral geniculate nucleus; vLGN, ventral LGN.

(Figure 2B,C). Additionally, a region that lacked retinal arbors appeared to separate the vLGN and IGL in *vldlr*$^{-/-}$;*lrp8*$^{-/-}$ mutants (Figure 2B,C). Despite these similarities with retinogeniculate targeting in the absence of reelin, we were surprised to find that a well-defined set of retinal projections to the IGL persisted in *vldlr*$^{-/-}$;*lrp8*$^{-/-}$

**Table 1 Retinogeniculate projection in phenotypes in wild-type and mutant mice**

| Genotype | Smaller retino-recipient region of vLGN | Sparse retinal projections to IGL | Misrouted retinal axons exiting medial border of LGN | Ectopic retinal projections in dLGN |
|---|---|---|---|---|
| Control | - | - | - | - |
| | (0/11) | (0/11) | (0/11) | (0/11) |
| *reln*$^{rl/rl}$ | ++ | ++ | ++ | - |
| | 7/7 | (7/7) | (7/7) | (0/7) |
| *vldlr*$^{-/-}$ | - | - | - | +/– |
| | (0/11) | (0/11) | (0/11) | (2/11) |
| *lrp8*$^{-/-}$ | - | - | - | - |
| | (0/9) | (0/9) | (0/9) | (0/9) |
| *vldlr*$^{+/-}$;*lrp8*$^{+/-}$ | - | - | - | - |
| | (0/9) | (0/9) | (0/9) | (0/9) |
| *vldlr*$^{+/-}$;*lrp8*$^{-/-}$ | - | + | - | + |
| | (0/6) | (2/6) | (0/6) | (2/6) |
| *vldlr*$^{-/-}$;*lrp8*$^{+/-}$ | +/– | + | +/– | + |
| | (4/7) | (3/7) | (1/7) | (5/7) |
| *vldlr*$^{-/-}$;*lrp8*$^{-/-}$ | ++ | ++ | +/– | ++ |
| | (7/7) | (7/7) | (2/7) | (7/7) |

The presence of four distinct defects in retinogeniculate projection patterns was assessed in various mutant mice: 1) small retinal projection patterns to vLGN; 2) a region of sparse retinal projections in or adjacent to IGL; 3) retinal axons misrouted out of the medial border of the vLGN and IGL; and 4) an ectopic region of binocular retinal projections in the dorsomedial pole of dLGN. Phenotypes were scored as being: –, absent; +/–, weak and only occasionally present; +, strong but only occasionally present; and ++, strong and highly penetrant. Parentheses indicate the number of mice exhibiting a phenotype compared to the total number of mice analyzed for that genotype. All mice included in these analyses ranged in age from P9 to P23. dLGN, dorsal LGN; IGL, intergeniculate leaflet; LGN, lateral geniculate nucleus; vLGN, ventral LGN.

mutants and very few retinal axons were observed exiting the medial border of the double mutant vLGN or IGL (Figure 2B,C and Table 1). In the few *vldlr*$^{-/-}$;*lrp8*$^{-/-}$ mutants (two out of six) where such misrouted axons were observed they were seen only in a small number of coronal LGN sections and were typically single axons that extended less than 100 μm from the LGN. These rare misrouted axons differed dramatically from the consist bundles of misrouted axons observed in *reln*$^{rl/rl}$ mutants that extend for several hundred microns outside of the LGN (see Figure 1B).

Unexpectedly, two defects were observed in retinal projections in *vldlr*$^{-/-}$;*lrp8*$^{-/-}$ mutants that we failed to observe in the >20 *reln*$^{rl/rl}$ mutants we have previously analyzed. First, dense patches of retinal arbors originating from the contralateral eye were directly adjacent to, and in some cases embedded within, the optic tract (see arrowheads in Figure 2B,C). Second, an ectopic patch of retinal arbors was present in the dorsomedial pole of dLGN (see asterisks in Figure 2B,C). Although this region of ectopic innervation was most commonly observed in the dorsomedial pole of mutant dLGN, it appeared to invade a more lateral portion of dLGN in extreme rostral sections of mutant LGN (Figure 3). Retinal arbors in these ectopic regions of innervation originated from both contra- and ipsilateral retinas, and were not segregate into eye-specific domains.

In the process of generating *vldlr*$^{-/-}$;*lrp8*$^{-/-}$ mutants, a large number of single reelin receptor gene mutants were generated that carried only one copy of the other canonical reelin receptor (*vldlr*$^{-/-}$;*lrp8*$^{+/-}$ and *vldlr*$^{+/-}$;*lrp8*$^{-/-}$ mice). We analyzed retinal projections in these mice to test the affect of gene dosage of these receptors on retinal targeting. All of the defective phenotypes described above for double mutants were observed in mutant heterozygote mice, although phenotypes were typically not as dramatic and not as penetrant as in double mutants (Table 1).

### Deletion of both VLDLR and LRP8 misroutes retinal axons to the dorsomedial pole of dLGN

We next set out to understand the mechanisms that underlie the formation of the ectopic, binocularly innervated region of dorsomedial dLGN in *vldlr*$^{-/-}$;*lrp8*$^{-/-}$ mutants. At perinatal ages (P3 to P4) projections from both eyes form diffuse, overlapping arbors in wild-type dLGN and vLGN. Similar diffuse projections were observed from ipsi- and contralateral retinas in *vldlr*$^{-/-}$ mutants, *lrp8*$^{-/-}$ mutants, and *vldlr*$^{-/-}$;*lrp8*$^{-/-}$ double mutants (Figure 4). Two striking defects were observed in retinal projections at perinatal ages in *vldlr*$^{-/-}$;*lrp8*$^{-/-}$ mutants. First, a lack of arbors was observed in the region separating the IGL and vLGN, similar to projections in *reln*$^{rl/rl}$ mutants at this age (although no axons were observed

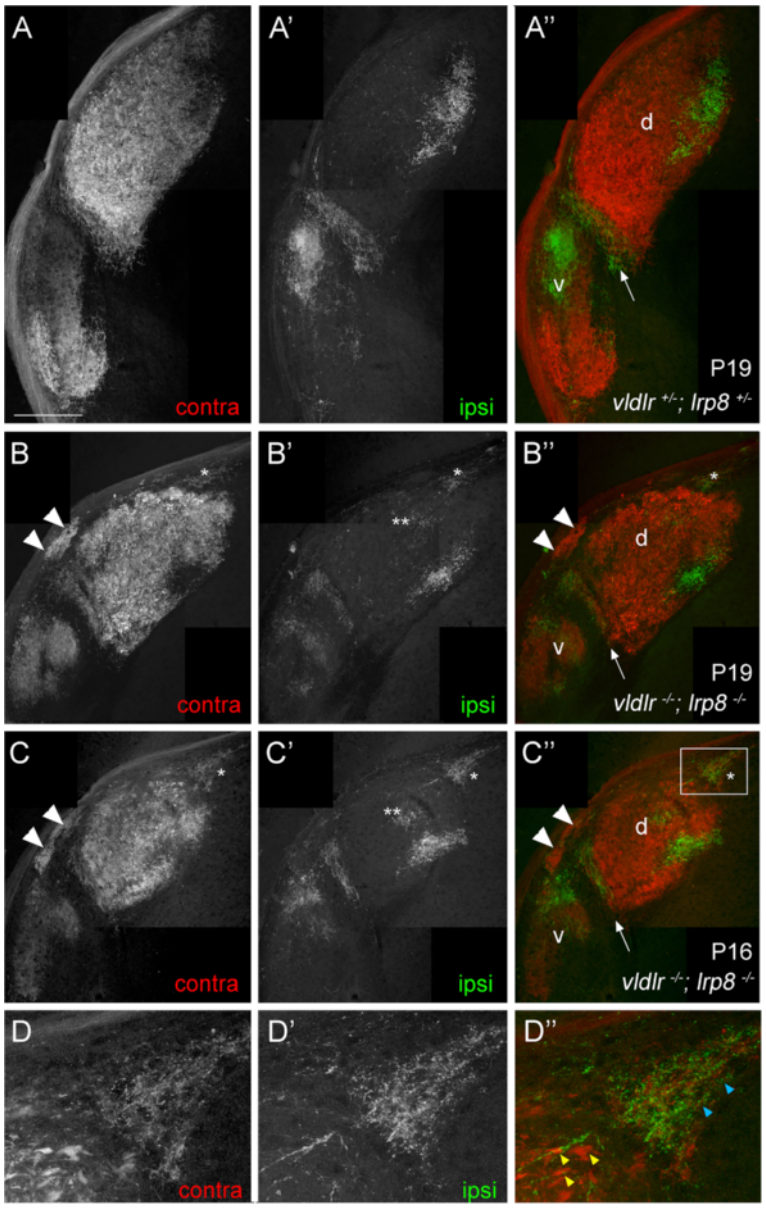


**Figure 2 Deletion of both VLDLR and LRP8 results in dramatic defects in retinogeniculate projections.** Retinogeniculate projections in **(A)** P19 control, **(B)** P19 *vldlr*$^{-/-}$;*lrp8*$^{-/-}$ double mutant and **(C)** P16 *vldlr*$^{-/-}$;*lrp8*$^{-/-}$ double mutant mice were labeled by intraocular injection of fluorescently conjugated CTB. In *vldlr*$^{-/-}$;*lrp8*$^{-/-}$ double mutants (**B**,**C**), note the absence of projection between the IGL and vLGN, the ectopic clusters of retinal arbors adjacent to the optic tract (arrowheads), and the ectopic region of binocular retinal input in the dorsomedial pole of the dLGN (asterisks). Double asterisks (**) indicate regions where retinal arbors from the ipsilateral retina have not been fully refined into segregated, eye-specific domains. **(D)** High magnification views of the boxed region in (**C**). Blue and yellow arrowheads in (**D**) highlight differences in retinal terminal size in dLGN (yellow) and the ectopic region at the dorsomedial pole of dLGN (blue). Left eyes were injected with Alexa Fluor 594 CTB and right eyes were injected with Alexa Fluor 488 CTB. LGN from right hemispheres are shown. 'Contra' denotes projections originating from the contralateral retina and 'ipsi' denotes projections originating from the ipsilateral retina. dLGN are labeled 'd', vLGN are labeled 'v' and arrows indicate IGL. The color of the label in panels (**A** to **D**) and (**A'** to **D'**) indicates the color of the image shown in (**A"** to **D"**). Scale bar = 200 μm for (**A** to **C**) and 75 μm for (**D**). CTB, cholera toxin B subunit; dLGN, dorsal LGN; IGL, intergeniculate leaflet; LGN, lateral geniculate nucleus; LRP8, low-density lipoprotein receptor-related protein 8; VLDLR, very-low-density lipoprotein receptor; vLGN, ventral LGN.

exiting the medial border of vLGN and IGL in *vldlr*$^{-/-}$;*lrp8*$^{-/-}$ mutants (n = 3)). Second, retinal axons appeared to innervate a distinct patch of thalamus that was dorsal to the dLGN in *vldlr*$^{-/-}$;*lrp8*$^{-/-}$ mutants (Figure 4D,F). Projections to this ectopic region originated from both ipsi- and contralateral retinas. These findings supported the notion that retinal axons were initially mistargeted into the dorsomedial pole of dLGN in *vldlr*$^{-/-}$;*lrp8*$^{-/-}$ mutants.

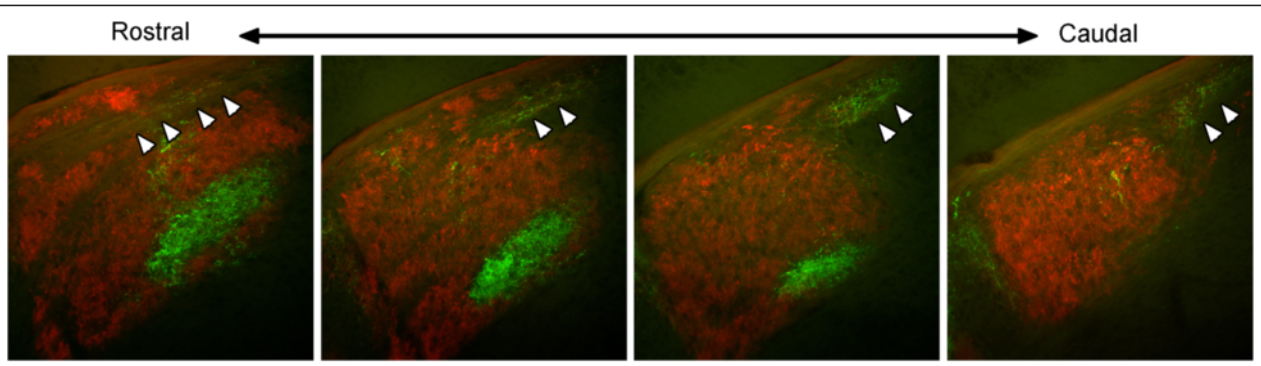


**Figure 3 Retinogeniculate projections in rostral and caudal sections of *vldlr*$^{-/-}$;*lrp8*$^{-/-}$ dLGN.** Retinogeniculate projections in a P16 *vldlr*$^{-/-}$; *lrp8*$^{-/-}$ mutant were labeled by intraocular injection of fluorescently conjugated CTB. The left eye was injected with Alexa Fluor 594 CTB and the right eye was injected with Alexa Fluor 488 CTB. Several sections of the same LGN from rostral to caudal are shown. Projections originating from the contralateral retina are labeled in red and projections originating from the ipsilateral retina are labeled in green. Arrowheads indicate regions of binocular, abnormal retinal projections. In central and caudal LGN sections, this region of ectopic innervation is in the dorsomedial pole of mutant dLGN. However, in extreme caudal sections, the ectopic innervation invades more lateral dLGN regions. Scale bar = 200 μm. CTB, cholera toxin B subunit; dLGN, dorsal LGN; LGN, lateral geniculate nucleus.

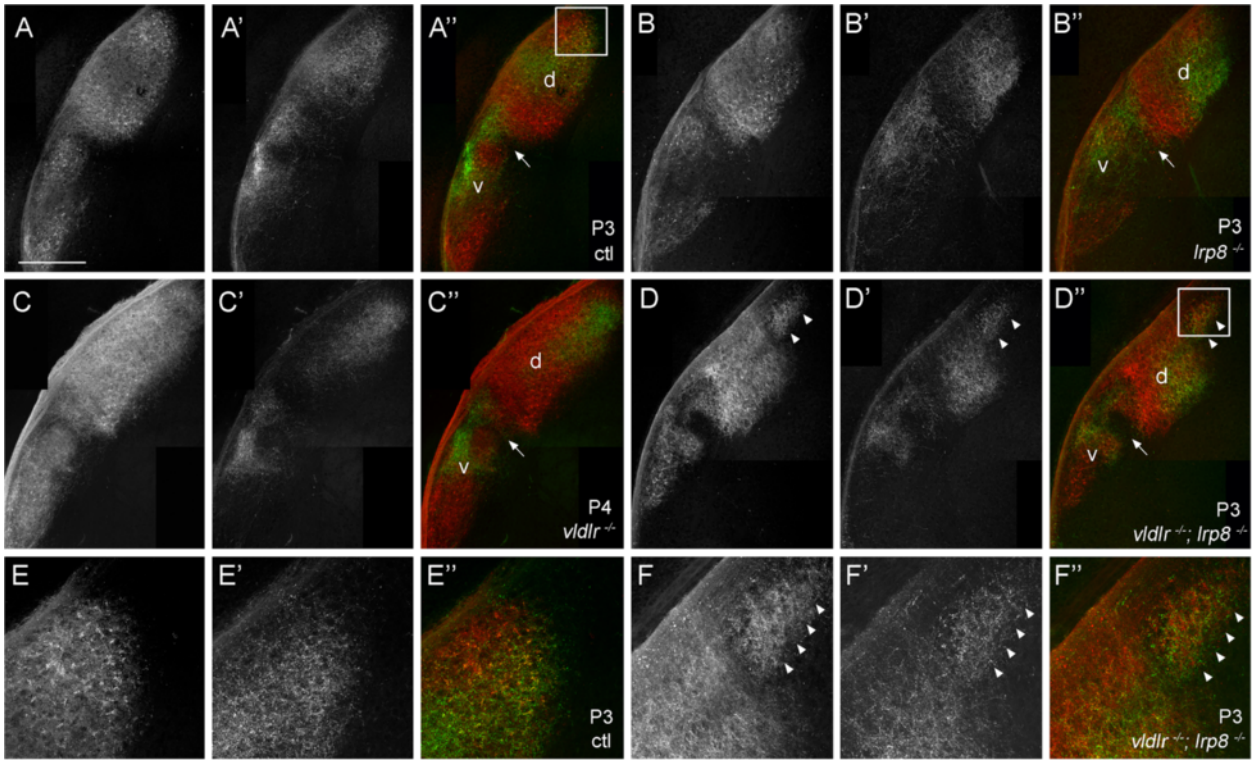


**Figure 4 Development of retinogeniculate projections in wild-type, *vldlr*$^{-/-}$, *lrp8*$^{-/-}$ and *vldlr*$^{-/-}$;*lrp8*$^{-/-}$mice.** Retinogeniculate projections in **(A)** P3 controls, **(B)** P3 *lrp8*$^{-/-}$ mutants, **(C)** P4 *vldlr*$^{-/-}$ mutants and **(D)** P3 *vldlr*$^{-/-}$;*lrp8*$^{-/-}$ mutants were labeled by intraocular injection of fluorescently conjugated CTB. In (**D**), note the ectopic region of binocular retinal input in the dorsomedial pole of *vldlr*$^{-/-}$;*lrp8*$^{-/-}$ dLGN is labeled with arrowheads. **(E,F)** High magnification images of the areas indicated by boxes in (**A**) and (**D**), respectively. Left eyes were injected with Alexa Fluor 594 CTB and right eyes were injected with Alexa Fluor 488 CTB. LGN from right hemispheres are shown. 'Contra' denotes projections originating from the contralateral retina and 'ipsi' denotes projections originating from the ipsilateral retina. dLGN are labeled 'd', vLGN are labeled 'v' and arrows indicate IGL. The color of the label in panels (**A** to **D**) and (**A'** to **D'**) indicates the color of the image shown in (**A"** to **D"**). Scale bar = 200 μm for (**A** to **D**) and 75 μm for (**E**,**F**). CTB, cholera toxin B subunit; dLGN, dorsal LGN; IGL, intergeniculate leaflet; LGN, lateral geniculate nucleus; vLGN, ventral LGN.

Further support for the idea that retinal axons were misrouted into the dorsomedial pole of dLGN in double mutants came from two observations regarding the morphology of CTB-labeled terminals in the ectopic patch of retinal innervation in dLGN. First, as noted above, retinal arbors appeared unsegregated based upon their eye of origin, a feature normally common only to those arbors within the IGL. Second, terminals in the dorsomedial pole of double mutant dLGN appeared morphologically smaller than other retinal terminals in dLGN (Figure 2D). We verified this result by labeling retinal terminals with antibodies against vesicular glutamate transporter 2 (VGluT2), a synaptic vesicle-associated protein whose distribution in LGN is restricted to retinal terminals [37]. Importantly, VGluT2 is specifically enriched in terminals and is largely absent from non-synaptic regions of axons. VGluT2-immunostaining revealed that retinal terminals in wild-type dLGN were considerably larger than their counterparts in vLGN and IGL (Figure 5A); and, as noted previously [38], the intensity of VGluT2-immnoreactivity was considerably less robust in wild-type IGL than in the adjacent vLGN and dLGN (Figure 5A). Similar differences in terminal size were observed in retinal terminals in vLGN, IGL and dLGN in *vldlr*$^{-/-}$;*lrp8*$^{-/-}$ mutants (Figure 5B). Analysis of the ectopic region of retinal innervation in the dorsomedial pole of *vldlr*$^{-/-}$;*lrp8*$^{-/-}$ mutant dLGN revealed terminal size was morphologically and quantitatively similar to terminals in control vLGN and IGL rather than those in the dLGN (Figure 5C to J). Taken together with developmental analyses, these data suggest that the ectopic region of retinal innervation in *vldlr*$^{-/-}$;*lrp8*$^{-/-}$ mutants resulted from defects in axonal targeting and not from aberrant retinal refinement.

### Cytoarchitectural defects in the LGN of *vldlr*$^{-/-}$;*lrp8*$^{-/-}$ mutants

We next sought to understand if cytoarchitectural changes in the LGN of *vldlr*$^{-/-}$;*lrp8*$^{-/-}$ mutants might underlie mistargeting of retinal axons into the dorsomedial pole of dLGN. For this we assessed the expression of *a d*isintegrin *a*nd *m*etalloproteinase with *t*hrombo*s*pondin motif 15 (ADAMTS15). We previously identified *adamts15* mRNA as a reliable marker of dLGN neurons [31]. *In situ* hybridization confirmed the enrichment of *adamts15* mRNA in wild-type dLGN neurons, and its absence from vLGN and IGL (Figure 6A). In *vldlr*$^{-/-}$;*lrp8*$^{-/-}$ mutants, *adamts15* mRNA was similarly absent from vLGN and IGL, and enriched throughout much of the dLGN (Figure 6B). Importantly, however, it appeared absent from the dorsomedial pole of the mutant dLGN where ectopic retinal arbors were present (Figure 6B). This suggested that dLGN relay neurons were absent from this region of mutant dLGN. We confirmed these results with an antibody directed against non-phosphorylated neurofilaments (SMI32), which has previously been shown to specifically label relay neurons and their dendrites in mouse dLGN and vLGN (but not in IGL) [31,39]. Immunostaining of wild-type P14 LGN produced a characteristic label of dLGN and vLGN neuropil (Figure 6C). In *vldlr*$^{-/-}$;*lrp8*$^{-/-}$ mutants similar reactivity was noted, with two exceptions: 1) little, if any, SMI32-immunoreactivity (SMI32-IR) was observed in the dorsomedial pole of the double mutant dLGN (Figure 6D, see single asterisk); and 2) SMI32-IR neurons were observed extending into the medial border of the double mutant IGL (Figure 6D, see arrowhead).

To further confirm cytoarchitectural differences in the dorsomedial pole of *vldlr*$^{-/-}$;*lrp8*$^{-/-}$ mutant dLGN, we next assessed the presence of other types of nerve terminals present in dLGN. A large portion of inputs to dLGN arise from corticothalamic (CT) axons originating from layer VI of visual cortex [40]. Terminals from these CT axons contain the synaptic vesicle associated protein, vesicular glutamate transporter 1 (VGluT1) [37,41]. While dense populations of VGluT1-containing terminals were present throughout the dorsal thalamus and dLGN of *vldlr*$^{-/-}$;*lrp8*$^{-/-}$ mutants, they appeared absent from the dorsomedial pole of mutant dLGN (Figure 6F). Taken together, studies on the distribution of *adamts15* mRNA, SMI32-IR and VGluT1-containing terminals all suggest that the dorsomedial pole of *vldlr*$^{-/-}$;*lrp8*$^{-/-}$ mutant dLGN is cytoarchitecturally different than adjacent regions of dLGN.

Since dLGN relay neurons appeared absent from the dorsomedial pole of mutant dLGN, we next asked whether any neurons were present in this region. Indeed, neuronal nuclei (NeuN) immunolabeling (which labels most neurons in mouse brain) revealed a normal density of neurons in mutant dLGN, including its dorsomedial pole (Figure 7A,B,C). Since neurons in the mutant dorsomedial pole lacked relay neuron markers we asked what their identity might be. First, we applied riboprobes against synaptotagmin 2 mRNA (*syt2*), a marker of vLGN neurons [31], to assess whether neurons in the dorsomedial pole of mutant dLGN may be derived from the vLGN. No *syt2*-expressing neurons were detected in the dorsomedial pole of mutant dLGN (data not shown). Next, we addressed whether these displaced neurons might be from the IGL, a possibility that seemed reasonable since IGL neurons do not express *adamts15* mRNA and are not labeled by SMI32 antibodies [31]. Additionally, aberrant retinal projections in the mutant dorsomedial dLGN pole fail to segregate into eye-specific domains and generate relatively small terminals, both features of retinal inputs to the IGL. To test our hypothesis we assessed the distribution of neuropeptide Y (NPY) in *vldlr*$^{-/-}$;*lrp8*$^{-/-}$ mutant LGN. In wild-type LGN, NPY-expressing neurons

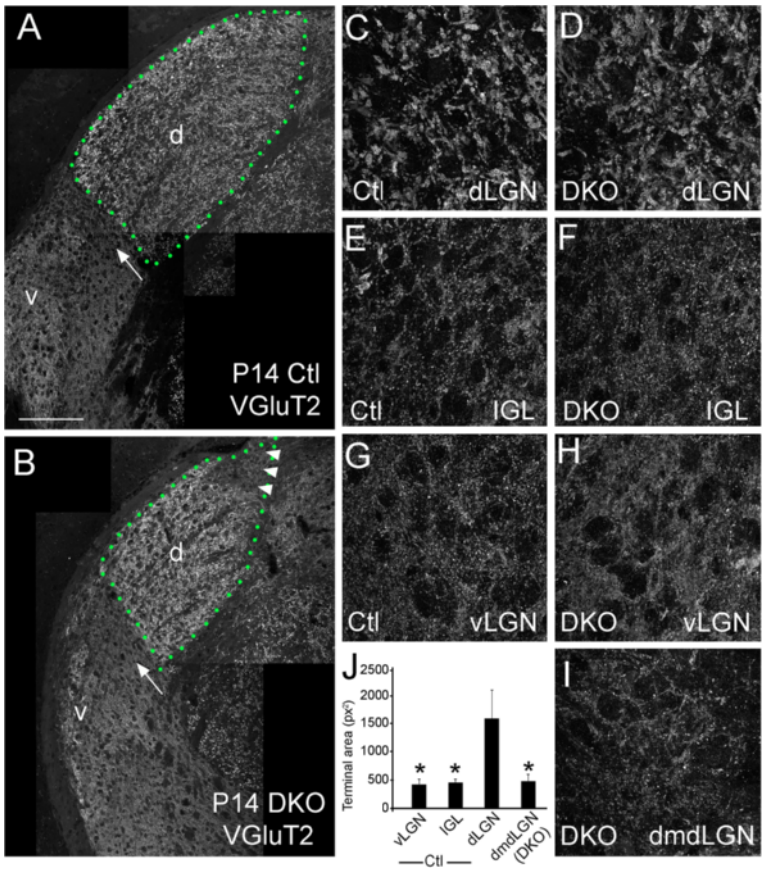


**Figure 5 Retinal terminals are smaller in the dorsomedial pole of *vldlr*$^{-/-}$;*lrp8*$^{-/-}$dLGN than throughout the rest of the dLGN.** Retinal terminals were labeled in **(A)** P14 control and **(B)** *vldlr*$^{-/-}$;*lrp8*$^{-/-}$ mutant (DKO) LGN by VGluT2-immunostaining. In (**B**), note the ectopic region of binocular retinal input in the dorsomedial pole of *vldlr*$^{-/-}$;*lrp8*$^{-/-}$ dLGN is labeled with arrowheads. **(C to I)** High magnification images of VGluT2-labeled terminals in control and mutant dLGN, IGL and vLGN. VGluT2-immunolabeled terminals in the dorsomedial pole of mutant dLGN (dmdLGN) are shown in (**I**). Note that the size of VGluT2-containing terminals in dorsomedial pole of mutant dLGN are dramatically smaller than those in dLGN (**C**,**D**) and instead appear similar to terminals in vLGN and IGL (**E**,**F**). **(J)** Terminals sizes were measured in ImageJ. Terminal areas (in pixels$^2$) were significantly larger in dLGN than in vLGN or IGL in controls. Terminal sizes in dorsomedial pole of mutant dLGN of DKO appeared quantitatively similar to control vLGN and IGL. $P$ <0.05 for terminal sizes in vLGN (control), IGL (control) and dorsomedial pole of mutant dLGN (DKO) compared with dLGN (control) by ANOVA. Differences in terminal size between vLGN (control), IGL (control) and dorsomedial pole of mutant dLGN (DKO) were not statistically significant. The outline of the dLGN is depicted with green dots. dLGN are labeled 'd', vLGN are labeled 'v' and arrows indicate IGL. Scale bar = 160 μm for (**A**,**B**) and 30 μm for (**C** to **I**). Ctl, control; DKO, double knockout; dLGN, dorsal LGN; dmdLGN, dorsomedial pole of mutant dLGN; IGL, intergeniculate leaflet; LGN, lateral geniculate nucleus; VGluT2, vesicular glutamate transporter 2; vLGN, ventral LGN.

are present in the IGL and are absent from all other adjacent thalamic regions (Figure 7A,D). In *vldlr*$^{-/-}$;*lrp8*$^{-/-}$ mutants, NPY-expression was present in IGL (although it appeared less organized than in controls), but was also present in vLGN and in the dorsomedial pole of the dLGN (Figure 7B,C,E,F). These results reveal that IGL neurons are malpositioned in the dorsomedial pole of the dLGN in *vldlr*$^{-/-}$;*lrp8*$^{-/-}$ mutants.

These data suggest that classes of IGL projecting retinal axons may target the dorsomedial pole of *vldlr*$^{-/-}$;*lrp8*$^{-/-}$ mutant dLGN due to the presence of malpositioned IGL neurons. Based on our previous findings that indicated reelin was a class-specific targeting cue for these axons, we next addressed whether reelin distribution was altered in *vldlr*$^{-/-}$;*lrp8*$^{-/-}$ mutants. Reelin immunostaining was performed on coronal sections of P3 *vldlr*$^{-/-}$;*lrp8*$^{-/-}$ mutant and littermate control brains. In every mutant examined (n = 3) reelin-expressing cells were observed in the dorsomedial pole of dLGN, as well as in regions of dLGN directly adjacent to the optic tract (Figure 8).

## Discussion

At the onset of these studies we hypothesized that deletion of both VLDLR and LRP8 would result in defects in retinogeniculate targeting that phenocopied those observed in *reln*$^{rl/rl}$ mutants. At first glance at least three features of retinal targeting in the LGN subnuclei appeared similar in both sets of mutant mice. The size of retinal

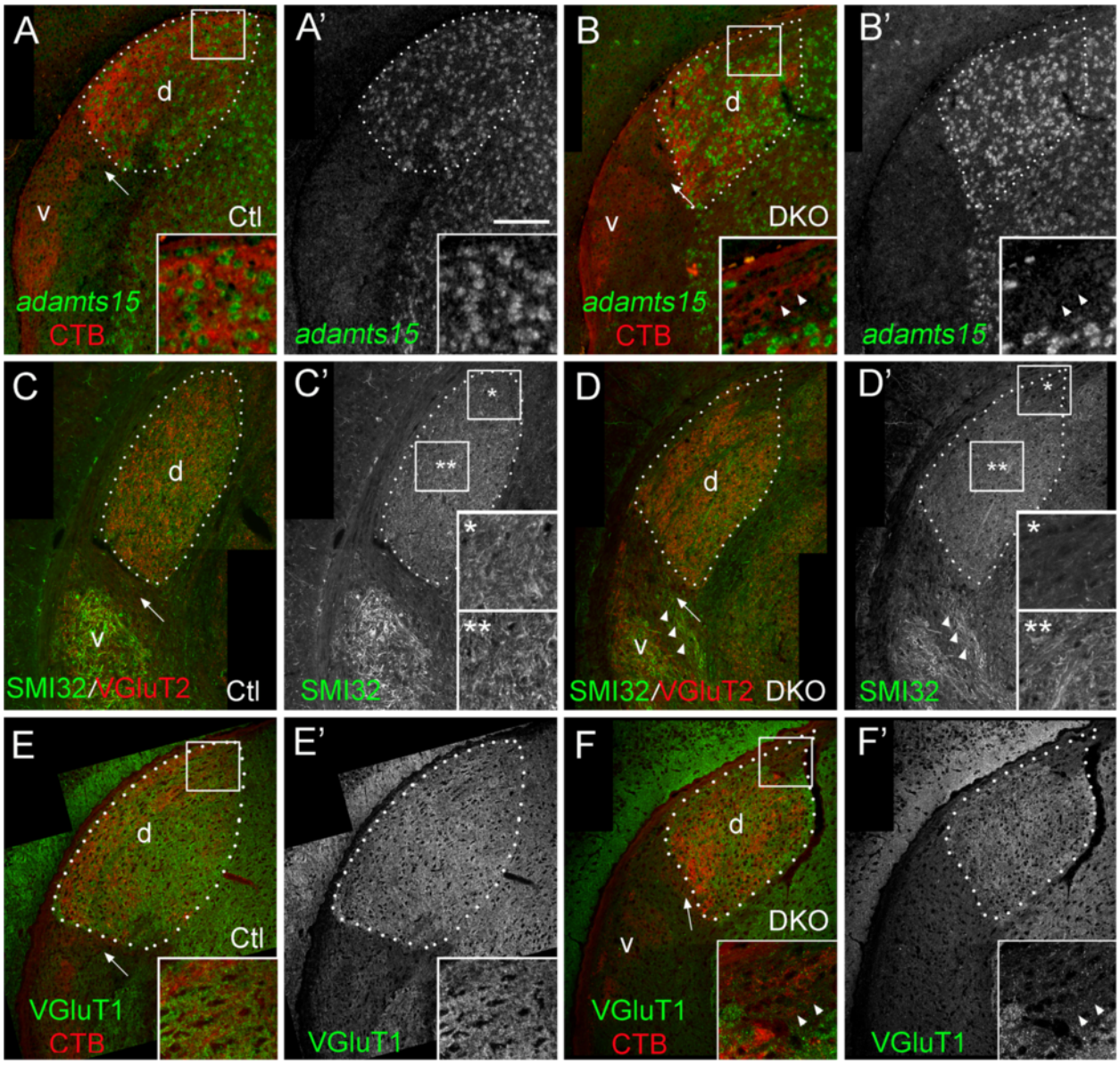


**Figure 6 Abnormal cytoarchitecture of the dorsomedial pole of *vldlr*$^{-/-}$;*lrp8*$^{-/-}$mutant dLGN.** *Adamts15* mRNA, which is expressed by thalamic relay neurons, was labeled by *in situ* hybridization in **(A)** P14 control and **(B)** *vldlr*$^{-/-}$;*lrp8*$^{-/-}$ mutant (DKO) LGN. Retinal arbors were labeled by binocular injection of Alexa Fluor 594 CTB. In (**B**), note the ectopic region of binocular retinal input in the dorsomedial pole of *vldlr*$^{-/-}$;*lrp8*$^{-/-}$ dLGN is labeled with arrowheads. Insets in (**A**,**B**) show high magnification images of the areas indicated by boxes. **(C,D)** dLGN and vLGN relay neurons (and their dendrites) were labeled by SMI32-immunostaining and retinal terminals were labeled by VGluT2-IHC. Note the absence of SMI32-immunoreactivity in the dorsomedial pole of *vldlr*$^{-/-}$;*lrp8*$^{-/-}$ mutant dLGN (asterisk). Also note the abnormal presence of SMI32-IR structures in *vldlr*$^{-/-}$;*lrp8*$^{-/-}$ mutant IGL (arrowheads). Insets in (**C**,**D**) show high magnification images of the areas indicated by boxes, and single and double asterisks. **(E,F)** Corticothalamic terminals in control and mutant dLGN were labeled by VGluT1-IHC. Retinal arbors were labeled by binocular injection of Alexa Fluor 594 CTB. In (**F**), note the absence of VGluT1-immunoreactivity in the dorsomedial pole of *vldlr*$^{-/-}$;*lrp8*$^{-/-}$ mutant dLGN (arrowheads). Insets in (**E**,**F**) show high magnification images of the areas indicated by boxes. For all images, the outline of the dLGN is depicted with white dots. dLGN are labeled 'd', vLGN are labeled 'v' and arrows indicate IGL. Scale bar = 180 μm for (**A** to **F**) and 50 μm for insets. CTB, cholera toxin B subunit; Ctl, control; DKO, double knockout; dLGN, dorsal LGN; IGL, intergeniculate leaflet; LGN, lateral geniculate nucleus; SMI32-IR, SMI32-immunoreactivity; VGluT1-IHC, vesicular glutamate transporter 1-immunohistochemistry; vLGN, ventral LGN.

projections to vLGN appeared reduced in *vldlr*$^{-/-}$;*lrp8*$^{-/-}$ mutants (Figure 2B,C), a defect previously noted in mutants lacking either reelin or functional DAB1 (Figure 1B) [31]. In all of these cases it remains unresolved if these defects reflect reduced numbers of retinal axons targeting vLGN, smaller terminal arbors of these axons, or smaller

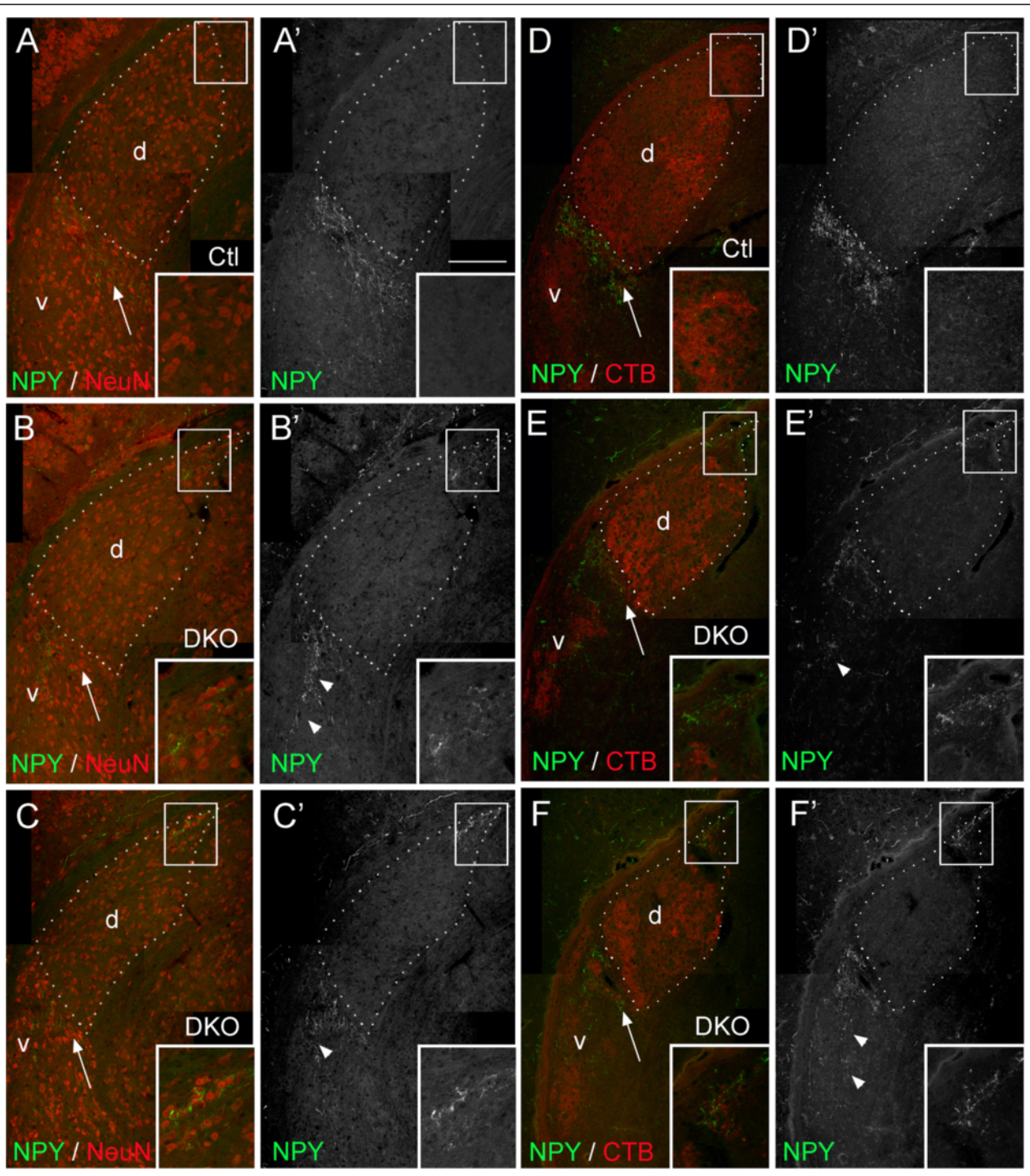


**Figure 7 Malposition of IGL neurons in *vldlr*$^{-/-}$;*lrp8*$^{-/-}$mutant LGN. (A,B)** NPY-expressing neurons, which are normally restricted to the IGL, were immunolabeled in **(A,D)** P14 control and **(B,C,E,F)** *vldlr*$^{-/-}$;*lrp8*$^{-/-}$ mutant (DKO) LGN. In (**A** to **C**), LGN neurons were colabeled by NeuN-IHC. In (**D** to **F**), retinal arbors were colabeled by binocular injection of Alexa Fluor 594 CTB. Insets show high magnification images of the boxed areas in (**A** to **F**). Note the presence of NPY-immunoreactivity in the dorsomedial pole of *vldlr*$^{-/-}$;*lrp8*$^{-/-}$ mutant dLGN (as seen in insets). NPY-immunoreactivity also extended into the vLGN in *vldlr*$^{-/-}$;*lrp8*$^{-/-}$ mutant LGN (arrowheads). For all images, the outline of the dLGN is depicted with white dots. dLGN are labeled 'd', vLGN are labeled 'v' and arrows indicate IGL. Scale bar = 180 μm for (**A** to **F**) and 50 μm for insets. CTB, cholera toxin B subunit; DKO, double knockout; dLGN, dorsal LGN; IGL, intergeniculate leaflet; IHC, immunohistochemistry; LGN, lateral geniculate nucleus; Neu-N; neuronal nuclei; NPY, neuropeptide Y; vLGN, ventral LGN.

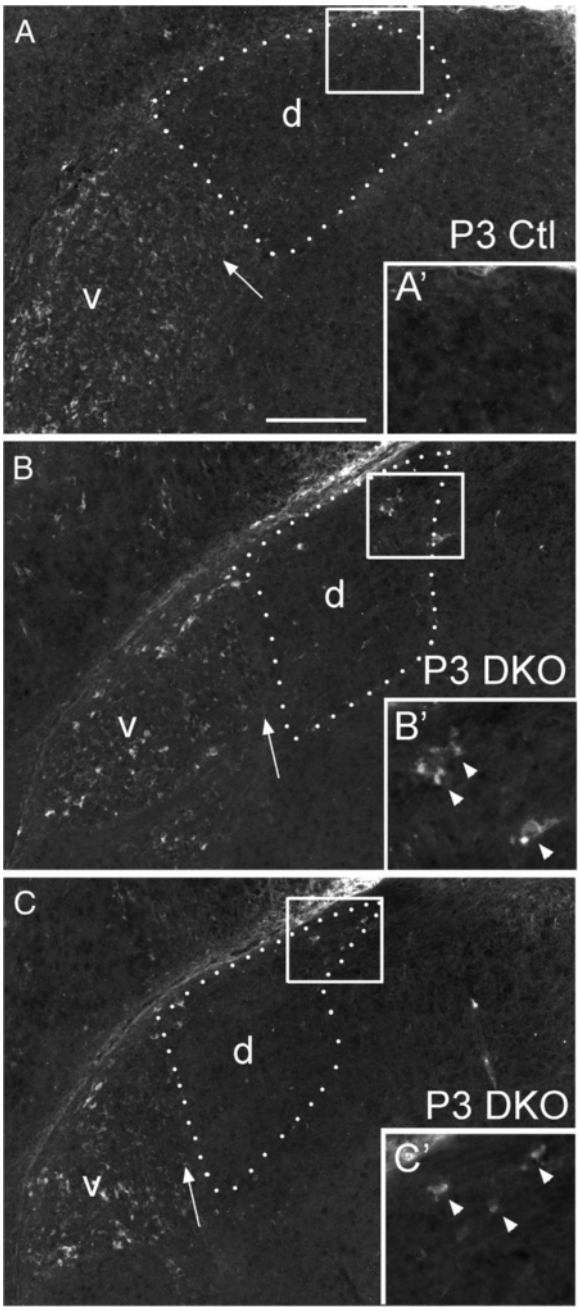


**Figure 8 Ectopic distribution of reelin in *vldlr*$^{-/-}$;*lrp8*$^{-/-}$mutant LGN.** Reelin distribution was assessed by immunostaining **(A)** P3 control and **(B,C)** *vldlr*$^{-/-}$;*lrp8*$^{-/-}$ mutant (DKO) LGN. Insets show high magnification images of the areas indicated by boxes. Note in (**B**,**C**), the presence of reelin-immunoreactivity in the dorsomedial pole of DKO mutant dLGN. For all images, the outline of the dLGN is depicted with white dots. dLGN are labeled 'd', vLGN are labeled 'v' and arrows indicate IGL. Scale bar = 180 μm for (**A** to **F**) and 50 μm for insets. DKO, double knockout; dLGN, dorsal LGN; IGL, intergeniculate leaflet; LGN, lateral geniculate nucleus; vLGN, ventral LGN.

retino-recipient nuclei. We also observed an absence of retinal arbors in and adjacent to the IGL in *vldlr*$^{-/-}$;*lrp8*$^{-/-}$ mutants. Similar uninnervated regions of LGN were observed in all reeler mutants examined and were present in some, but not all, DAB1 mutants [31]. Despite outward similarities in these two phenotypes in *vldlr*$^{-/-}$; *lrp8*$^{-/-}$, *reln*$^{rl/rl}$ and *dab1*$^{scm/scm}$ mutant LGN, it is important to point out some minor differences. First, the penetrance and strength of these two phenotypes were reduced in receptor mutants compared with those observed in mutants lacking reelin (Table 1). The penetrance and strength was similarly reduced in *dab1*$^{scm/scm}$ mutants [31] (unpublished data); however, a small amount of residual DAB1 protein remains present in these spontaneously generated mutant mice raising the question of whether penetrance issues arise from incomplete removal of DAB1. Second, in contrast to *reln*$^{rl/rl}$ mutants, an organized set of projections to IGL remained present (albeit reduced) in *vldlr*$^{-/-}$;*lrp8*$^{-/-}$ mutants (compare IGL in Figure 1B and [31] with those in Figures 2B,C). Third, cytoarchitectural analysis revealed differences in the molecular and cellular make-up of LGN subnuclei in *vldlr*$^{-/-}$;*lrp8*$^{-/-}$ and *reln*$^{rl/rl}$ mutants, a feature that complicates comparisons of the retinogeniculate projection phenotypes described above. Specifically, our studies demonstrated that SMI32-IR neurons abnormally invaded IGL in the absence of VLDLR and LRP8 (Figure 6), a phenotype not observed in mutants lacking reelin [31]. Additionally NPY neurons, which normally reside only in the IGL, migrate into the vLGN and dLGN in the absence of VLDLR and LRP8 but not in the absence of reelin (Figure 7) [31]. These results are summarized in Figure 9.

The final similarity in abnormal retinal projections in *vldlr*$^{-/-}$;*lrp8*$^{-/-}$ and *reln*$^{rl/rl}$ mutants is an incomplete refinement of retinal terminals into eye-specific domains (Figure 9), an essential feature in the establishment of visual system circuits [1,42]. Impaired refinement of retinal projections was also observed in *dab1*$^{scm/scm}$, *vldlr*$^{-/-}$, and *lrp8*$^{-/-}$ mutants (Figure 1C,D and data not shown). Since refinement of eye-specific arbors requires retinal activity, defects in eye-specific segregation is not entirely unexpected in these mutants. Retinal activity has previously been shown to be perturbed in the absence of reelin, DAB1, VLDLR or LRP8 [43,44].

Despite the above described similarities in retinal projections in *vldlr*$^{-/-}$;*lrp8*$^{-/-}$ and *reln*$^{rl/rl}$ mutants, two more notable differences in phenotypes were observed in our studies. First, the deletion of both canonical reelin receptors largely failed to generate bundles of misrouted retinal axons that exited the medial borders of the vLGN and IGL, and invaded non-retino-recipient regions of thalamus. Misrouting of axons from ipRGCs into medial thalamus was a distinguishing feature of retinal

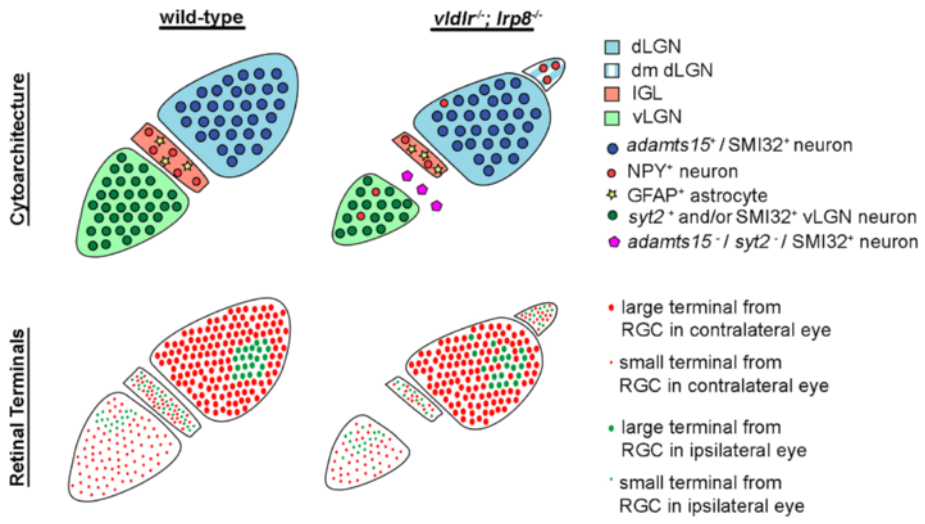


**Figure 9 VLDLR and LRP8 contribute to the cytoarchitecture and retinal targeting of mouse LGN.** A diagram summarizing defects in cytoarchitecture and retinal terminal distribution in mutant mice lacking both VLDLR and LRP8. dmdLGN, dorsomedial pole of dLGN; dLGN, dorsal LGN; IGL, intergeniculate leaflet; LGN, lateral geniculate nucleus; LRP8, low-density lipoprotein receptor-related protein 8; RGC, retinal ganglion cell; VLDLR, very-low-density lipoprotein receptor; vLGN, ventral lateral geniculate nucleus.

targeting in the absence of either reelin or DAB1 [20,31]. The lack of ipRGC axons erroneously exiting the medial border of IGL in *vldlr*$^{-/-}$;*lrp8*$^{-/-}$ mutants may help explain why projections to the IGL in these double mutants appears more developed than in *reln*$^{rl/rl}$ mutants. Second, an ectopic region of binocular retinal input was observed in the dorsomedial pole of *vldlr*$^{-/-}$;*lrp8*$^{-/-}$ LGN (Figure 9), a feature never observed in mutants lacking reelin or functional DAB1 [31]. Cytoarchitectural analyses demonstrated that NPY-expressing IGL neurons aberrantly migrate into this region of *vldlr*$^{-/-}$;*lrp8*$^{-/-}$ dLGN, and despite being displaced these cells generate a micro-domain that is uniquely distinct from surrounding dLGN and dorsal thalamus. Based on the density of NeuN-positive neurons in this micro-domain we suspect that additional types of non-NPY expressing classes of IGL neurons may also be present in this ectopic region. Certainly, reelin-expressing cells, which normally populate both IGL and vLGN [31], were present in this micro-domain of mutant dLGN. In wild-type tissue, a cohort of glial fibrillary acidic protein (GFAP)-expressing astrocytes also populate IGL but not the surrounding tissue [45]. Surprisingly, we failed to observe GFAP-immunoreactivity in the dorsomedial pole of *vldlr*$^{-/-}$;*lrp8*$^{-/-}$ mutant dLGN, suggesting that these cell populations were less affected by the loss of VLDLR and LRP8 (data not shown), and hinting that these glial cells are not the source of reelin in the IGL. Based on the presence of IGL target neurons and reelin in the dorsomedial pole of mutant dLGN, we posit that IGL-projecting classes of retinal axons are misrouted into this micro-domain of mutant dLGN. In support of this hypothesis, retinal arbors in this micro-domain remain unsegregated based on their eye of origin and form small terminals, two features that are hallmarks of retinal projections in wild-type IGL. Taken together, data presented here paint a picture that VLDLR and LRP8 have reelin-independent roles in the migration of IGL neurons during thalamic development. Likewise, the lack of misrouted ipRGC axons into medial thalamus suggests that reelin signals through other receptors for the establishment of class-specific retinogeniculate circuits.

What might these non-canonical reelin receptors be? Despite the plethora of studies on reelin's function in neural development and synaptic function few receptors other than VLDLR and LRP8 have been identified. Integrin α3β1 binds to the N-terminal f-spondin domain of reelin and can activate DAB1 in a reelin-dependent manner [46,47]. Since disruption in α3β1 signaling does not result in severe defects in neuronal position (like deletion of reelin or DAB1), it has been suggested that reelin-α3β1 integrin interactions may be more essential during neurite outgrowth, synapse formation or synaptic function [47-49]. Based on its established role in neurite extension [50,51] and expression in retinal axons [52], α3β1 integrin is a prime candidate to mediate the class-specific axon targeting function of reelin in mouse LGN. However, another prime candidate for mediating reelin's role in axon targeting in the visual system is amyloid precursor protein (APP), a transmembrane receptor with established roles in mediating neurite outgrowth [53,54] and synapse assembly [55]. APP binds to the central repeating domain of reelin (reelin repeats 3 to 6), an interaction that promotes neurite outgrowth [56]. These findings, together with the fact that APP is expressed by at least some mammalian RGCs [57],

make APP a reasonable candidate for mediating the class-specific axon targeting function of reelin in LGN. The last non-canonical reelin receptor that we shall discuss is the protocadherin cadherin-related neuronal receptor 1 (CNR1) [58]. CNR1 remains a controversial reelin binding partner [59,60], but due to isoform diversity and alternative splicing the cadherin superfamily (which includes classical cadherins, protocadherins, FAT-family cadherins, T-cadherins and 7TM-cadherins) [58] has been of particular interest for its role in the specific wiring of neural circuits [61,62]. Based upon the expression of many cadherins and protocadherins by RGCs, and the role of classical cadherins in RGC axon targeting [63-66], CNR1 is an intriguing candidate receptor for mediating the class-specific axon targeting function of reelin in LGN.

Finally, what non-reelin ligand might bind and activate VLDLR and LRP8 to affect neuronal migration during thalamic development? Since both VLDLR and LRP8 are members of the LDL family of lipoprotein receptors they can bind a variety of lipoproteins including compounds containing apolipoprotein E (ApoE). ApoE has been shown to affect cell migration in a variety of systems [67], suggesting it may be the LGN ligand for VLDLR and LRP8. However, other candidate extracellular ligands with known roles in cell migration have also been identified. Both canonical reelin receptors are also capable of binding thrombospondin (THBS), a bulky extracellular proteoglycan present in the developing brain [68,69]. Like reelin, binding of THBS to VLDLR and LRP8 activates DAB1, but the subsequent downstream signaling events differ from that of reelin induced signals [68]. Our previous studies identified an isoform of THBS, THBS4, as being one of the extracellular cues most significantly enriched in vLGN/IGL compared with dLGN at perinatal ages of mouse development [31]. Roles for thrombospondins in LGN development remain unresolved.

## Conclusions

Identifying the molecular underpinnings of class-specific targeting of axons to correct brain regions is essential for our understanding of how complex neural circuits are assembled. Visual system circuits are ideal models to study class-specific axonal targeting since there are over 20 distinct classes of RGCs in the mammalian retina, each with a unique stereotyped pattern of axonal projections to a cohort of retino-recipient nuclei within the brain [11-19,70-73]. Such diversity of neuronal subtypes and class-specific circuitry is not unique to the retina, but instead is a central feature of many regions of the mammalian brain. In a previous study we identified reelin, a bulky extracellular proteoglycan, as a critical molecular component required for the targeting of LGN subnuclei by distinct classes of retinal axons. Here we addressed whether this function of reelin required the two canonical reelin receptors, VLDLR and LRP8. While genetic deletion of either VLDLR or LRP8 had little affect on the initial targeting of retinal axons to LGN subnuclei (despite clear affects on the refinement of these axons into segregated, eye-specific domains), several defects were observed in retinal axon targeting in mutant mice lacking both receptors. However, in contrast to our hypothesis that reelin would utilize these receptors for class-specific retinogeniculate targeting, we found that deletion of both canonical reelin receptors failed to accurately phenocopy retinal targeting defects present in *reln*$^{rl/rl}$ mutant LGN. The misrouting of retinal axons into medial, non-retino-recipient thalamus in the absence of reelin were not observed in *vldlr*$^{-/-}$;*lrp8*$^{-/-}$ mutants and aberrant patterns of retinal projections seen in *vldlr*$^{-/-}$;*lrp8*$^{-/-}$ mutants (which appeared secondary to defects in neuronal migration) were not observed in mutants lacking reelin. We take these results to suggest that non-canonical reelin receptors contribute to reelin's role in retinogeniculate targeting, and other extracellular ligands activate VLDLR and LRP8 for the proper migration of IGL neurons.

## Methods

### Mice

Wild-type C57 mice were obtained from Charles River (Wilmington, MA, USA). Reeler mutant mice (*reln*$^{rl/rl}$), *vldlr*$^{-/-}$ and *lrp8*$^{-/-}$mice were obtained from The Jackson Laboratory (Bar Harbor, ME, USA). Genomic DNA was isolated from tail and genotyping performed as previously described [31,74-76]. The following primer pairs were used: *reln*, TTA ATC TGT CCT CAC TCT GCC CTC T and GCA GAC TCT CTT ATT GTC TCT AC; mutant *reln*, TTA ATC TGT CCT CAC TCT GCC CTC T and TTC CTC TCT TGC ATC CTG TTT TG [73]; *vldlr*, TGG TGA TGA GAG GCT TGT ATG TTG TC and TTG ACC TCA TCG CTG CCG TCC TTG; mutant *vldlr*, CGG CGA GGA TCT CGT CGT GAC CCA and GCG ATA CCG TAA AGC ACG AGG AAG; *lrp8*, CCA CAG TGT CAC ACA GGT AAT GTG and ACG ATG ACC CCA ATG ACA GCA GCG; mutant *lrp8*, GAT TGG GAA GAC AAT AGC AGG CAT GC and GCT TGT TGG AAT TCA GCC AGT TAC C. All analyses conformed to National Institutes of Health (NIH) guidelines and protocols, approved by the Virginia Polytechnic Institute and State University, and Virginia Commonwealth University (VCU) Institutional Animal Care and Use Committees.

### Antibodies

Antibodies for the following antigens were purchased: rabbit anti-VGluT2 and rabbit anti- VGluT1 (diluted 1:500; Synaptic Systems, Göttingen, Germany), mouse anti-reelin (diluted 1:1000; Abcam, Cambridge, UK), rabbit anti-NPY

(diluted 1:500; ImmunoStar, Hudson, WI, USA), mouse anti-NeuN (diluted 1:200; Millipore, Billerica, MA, USA), rabbit anti-glutamate decarboxylase 65/67 (GAD65/67) (diluted 1:500; Millipore Bioscience Research Reagents, Temecula, CA, USA), and mouse anti-SMI32 (diluted 1:500; Covance, Princeton, NJ, USA). Fluorescently conjugated secondary antibodies were purchased from Invitrogen (Carlsbad, CA, USA) or Jackson ImmunoResearch (diluted 1:1000; West Grove, PA, USA).

### Immunohistochemistry

Immunohistochemistry (IHC) was performed on 16 μm coronal cryosectioned tissues as previously described [31,38,74,76]. Briefly, tissue slides were allowed to air dry for 15 minutes before being incubated with blocking buffer (2.5% normal goat serum, 2.5% bovine serum albumin and 0.1% Triton X-100 in PBS) for 30 minutes. Primary antibodies were diluted in blocking buffer and incubated on tissue sections for overnight at 4°C. On the following day, tissue slides were washed in PBS and secondary antibodies diluted 1:1000 in blocking buffer were applied to slides for 1 hour at room temperature. After thoroughly washing in PBS, tissue slides were coverslipped with VectaShield (Vector Laboratories, Burlingame, CA, USA). Images were acquired on a Zeiss Axio Imager A2 fluorescent microscope, a Zeiss Examiner Z1 LSM 710 confocal microscope, or a Zeiss LSM 700 confocal microscope (Oberkochen, Germany). When comparing different ages of tissues or between genotypes, images were acquired with identical parameters. The size of VGluT2-immunoreactive retinal terminals was measured with ImageJ (NIH, Bethesda, MD, USA). The area of individual puncta in control and mutant vLGN, IGL and dLGN were measured manually. A minimum of three animals (per genotype and per age) was compared in all IHC experiments.

### *In situ* hybridization

*In situ* hybridization (ISH) was performed on 16 μm coronal cryosectioned tissues as previously described [31,74,76]. The generation of *adamts15* (clone IDs 30619053) riboprobes was previously described [31]. Briefly, riboprobes were synthesized using digoxigenin (DIG)-labeled UTP (Roche, Mannheim, Germany) and the MAXIscript In Vitro Transcription Kit (Ambion, Austin, TX, USA). Probes were hydrolyzed to 500 nt. Coronal brain sections were prepared and hybridized at 65°C as previously described (Su *et al*., 2010), and bound riboprobes were detected by horseradish peroxidase (POD)-conjugated anti-DIG antibodies and fluorescent staining with Tyramide Signal Amplification (TSA) systems (PerkinElmer, Shelton, CT, USA). Images were obtained on a Zeiss Axio Imager A2 fluorescent microscope or a Zeiss Examiner Z1 LSM 710 confocal microscope. A minimum of three animals per genotype and age was compared in ISH experiments.

### Intraocular injections of anterograde tracers

Intraocular injection of CTB conjugated to Alexa Fluor 488 or Alexa Fluor 594 (Invitrogen) was performed as previously described [31,39]. Briefly, mice were anesthetized with hypothermia (<P7) or by isoflurane vapors (>P7). The sclera was pierced with a sharp-tipped glass pipette and excess vitreous was drained. Another pipette, filled with a 0.1 to 0.2% solution of CTB, was inserted into the hole made by the first pipette. The pipette containing the CTB was attached to a picospritzer and a prescribed volume (1 to 3 μl at P3 to P10 and 3 to 5 μl for ages >P10) of solution was injected into the eye. After 1 to 2 days, mice were killed and brains were fixed in 4% paraformaldehyde. A total of 100 μm coronal sections were sectioned on a vibratome (Microm HM 650 V; Thermo Scientific, Waltham, MA, USA) and mounted in ProLong Gold (Invitrogen). Retinal projections were analyzed from between 3 to 12 animals for each age and genotype. Images were acquired on a Zeiss Examiner Z1 LSM 710 confocal microscope or a Zeiss LSM 700 confocal microscope. We documented four types of defects in retinogeniculate targeting in wild-type (control), *reln*$^{rl/rl}$, *vldlr*$^{-/-}$, *lrp8*$^{-/-}$, *vldlr*$^{-/-}$;*lrp8*$^{-/-}$, *vldlr*$^{-/-}$;*lrp8*$^{+/-}$ and *vldlr*$^{+/-}$; *lrp8*$^{-/-}$ mice: 1) smaller pattern of retinal projection to vLGN; 2) an absence of retinal axons between vLGN and IGL; 3) retinal axons abnormally exiting the medial border of the vLGN with IGL; and 4) retinal axons from both ipsilateral and contralateral retinas that ectopically innervate to the dorsomedial pole of dLGN. We scored these phenotypes objectively based on penetrance and subjectively based on robustness. All sections were scored blind by at least two observers.

#### Abbreviations

ADAMTS15: A disintegrin and metalloproteinase with thrombospondin type 1 motif member 15; ANOVA: Analysis of variance; ApoE: Apolipoprotein E; ApoER2: Apolipoprotein E receptor 2; APP: Amyloid precursor protein; CNR1: Cadherin-related neuronal receptor 1; CNS: Central nervous system; CT: Corticothalamic; CTB: Cholera toxin B subunit; DAB1: Disabled-1; DIG: Digoxigenin; DKO: Double knockout; dLGN: Dorsal LGN; dmdLGN: Dorsomedial pole of dLGN; EGF: Epidermal growth factor; GAD: Glutamate decarboxylase; GFAP: Glial fibrillary acidic protein; IGL: Intergeniculate leaflet; IHC: Immunohistochemistry; ipRGC: Intrinsically photosensitive RGC; ISH: *In situ* hybridization; LDL: Low-density lipoprotein; LGN: Lateral geniculate nucleus; LRP8: Low-density lipoprotein receptor-related protein 8; NeuN: Neuronal nuclei; NIH: National Institutes of Health; NPY: Neuropeptide Y; PBS: Phosphate-buffered saline; POD: Peroxidase; RGC: Retinal ganglion cell; SMI32-IR: SMI32-immunoreactivity; syt2: Synaptotagmin 2; THBS: Thrombospondin; TSA: Tyramide Signal Amplification; VCU: Virginia Commonwealth University; VGluT1: Vesicular glutamate transporter 1; VGluT2: Vesicular glutamate transporter 2; VLDLR: Very-low-density lipoprotein receptor; vLGN: Ventral LGN.

#### Competing interests

The authors declare that they have no competing interests.

**Authors' contributions**
JS carried out the collection, preparation and imaging of CTB injected tissues, performed IHC and ISH experiments, and helped draft portions of the manuscript. MAK carried out data collection and image analysis. AMJ carried out the collection, preparation and imaging of CTB injected tissues. MAF conceived, designed and coordinated the study, and drafted the manuscript. All authors read and approved the final version of the manuscript.

**Acknowledgements**
This work was supported by the NIH (EY021222) (MAF), the Thomas F Jeffress and Kate Miller Jeffress Memorial Trust (MAF), and the VCU Presidential Research Incentive Program (PRIP) (MAF). A small portion of the microscopy was performed at the VCU Microscopy Core supported, in part, with funding from NIH (NS047463).

**Author details**
[1]Virginia Tech Carilion Research Institute, Roanoke, VA 24016, USA. [2]Department of Biological Sciences, Virginia Tech, Blacksburg, VA 24061, USA. [3]Department of Anatomy and Neurobiology, Virginia Commonwealth University Medical Center, Richmond, VA 23298, USA.

Received: 24 February 2013 Accepted: 22 May 2013
Published: 13 June 2013

**References**

1. Huberman AD, Feller MB, Chapman B: **Mechanisms underlying development of visual maps and receptive fields.** *Annu Rev Neurosci* 2008, **31:**479–509.
2. Triplett JW, Feldheim DA: **Eph and ephrin signaling in the formation of topographic maps.** *Semin Cell Dev Biol* 2011, **23**(1):7–15.
3. Sanes JR, Yamagata M: **Many paths to synaptic specificity.** *Annu Rev Cell Dev Biol* 2009, **25:**161–195.
4. Pfeiffenberger C, Cutforth T, Woods G, Yamada J, Renteria RC, Copenhagen DR, Flanagan JG, Feldheim DA: **Ephrin-As and neural activity are required for eye-specific patterning during retinogeniculate mapping.** *Nat Neurosci* 2005, **8**(8):1022–1027.
5. Leamey CA, Merlin S, Lattouf P, Sawatari A, Zhou X, Demel N, Glendining KA, Oohashi T, Sur M, Fassler R: **Ten_m3 regulates eye-specific patterning in the mammalian visual pathway and is required for binocular vision.** *PLoS Biol* 2007, **5**(9):e241.
6. Rebsam A, Petros TJ, Mason CA: **Switching retinogeniculate axon laterality leads to normal targeting but abnormal eye-specific segregation that is activity dependent.** *J Neurosci* 2009, **29**(47):14855–14863.
7. Huh GS, Boulanger LM, Du H, Riquelme PA, Brotz TM, Shatz CJ: **Functional requirement for class I MHC in CNS development and plasticity.** *Science* 2000, **290**(5499):2155–2159.
8. Bjartmar L, Huberman AD, Ullian EM, Renteria RC, Liu X, Xu W, Prezioso J, Susman MW, Stellwagen D, Stokes CC, Cho R, Worley P, Malenka RC, Ball S, Peachey NS, Copenhagen D, Chapman B, Nakamoto M, Barres BA, Perin MS: **Neuronal pentraxins mediate synaptic refinement in the developing visual system.** *J Neurosci* 2006, **26**(23):6269–6281.
9. Stevens B, Allen NJ, Vazquez LE, Howell GR, Christopherson KS, Nouri N, Micheva KD, Mehalow AK, Huberman AD, Stafford B, Sher A, Litke AM, Lambris JD, Smith SJ, John SW, Barres BA: **The classical complement cascade mediates CNS synapse elimination.** *Cell* 2007, **131**(6):1164–1178.
10. Datwani A, McConnell MJ, Kanold PO, Micheva KD, Busse B, Shamloo M, Smith SJ, Shatz CJ: **Classical MHCI molecules regulate retinogeniculate refinement and limit ocular dominance plasticity.** *Neuron* 2009, **64**(4):463–470.
11. Hong YK, Kim IJ, Sanes JR: **Stereotyped axonal arbors of retinal ganglion cell subsets in the mouse superior colliculus.** *J Comp Neurol* 2011, **519**(9):1691–1711.
12. Kim IJ, Zhang Y, Yamagata M, Meister M, Sanes JR: **Molecular identification of a retinal cell type that responds to upward motion.** *Nature* 2008, **452**(7186):478–482.
13. Kim IJ, Zhang Y, Meister M, Sanes JR: **Laminar restriction of retinal ganglion cell dendrites and axons: subtype-specific developmental patterns revealed with transgenic markers.** *J Neurosci* 2010, **30**(4):1452–1462.
14. Huberman AD, Manu M, Koch SM, Susman MW, Lutz AB, Ullian EM, Baccus SA, Barres BA: **Architecture and activity-mediated refinement of axonal projections from a mosaic of genetically identified retinal ganglion cells.** *Neuron* 2008, **59**(3):425–438.
15. Huberman AD, Wei W, Elstrott J, Stafford BK, Feller MB, Barres BA: **Genetic identification of an On-Off direction-selective retinal ganglion cell subtype reveals a layer-specific subcortical map of posterior motion.** *Neuron* 2009, **62**(3):327–334.
16. Rivlin-Etzion M, Zhou K, Wei W, Elstrott J, Nguyen PL, Barres BA, Huberman AD, Feller MB: **Transgenic mice reveal unexpected diversity of on-off direction-selective retinal ganglion cell subtypes and brain structures involved in motion processing.** *J Neurosci* 2011, **31**(24):8760–8769.
17. Yonehara K, Shintani T, Suzuki R, Sakuta H, Takeuchi Y, Nakamura-Yonehara K, Noda M: **Expression of SPIG1 reveals development of a retinal ganglion cell subtype projecting to the medial terminal nucleus in the mouse.** *PLoS One* 2008, **3**(2):e1533.
18. Yonehara K, Ishikane H, Sakuta H, Shintani T, Nakamura-Yonehara K, Kamiji NL, Usui S, Noda M: **Identification of retinal ganglion cells and their projections involved in central transmission of information about upward and downward image motion.** *PLoS One* 2009, **4**(1):e4320.
19. Hattar S, Kumar M, Park A, Tong P, Tung J, Yau KW, Berson DM: **Central projections of melanopsin-expressing retinal ganglion cells in the mouse.** *J Comp Neurol* 2006, **497**(3):326–349.
20. Fox MA, Guido W: **Shedding light on class-specific wiring: development of intrinsically photosensitive retinal ganglion cell circuitry.** *Mol Neurobiol* 2011, **44**(3):321–329.
21. D'Arcangelo G, Miao GG, Chen SC, Soares HD, Morgan JI, Curran T: **A protein related to extracellular matrix proteins deleted in the mouse mutant reeler.** *Nature* 1995, **374**(6524):719–723.
22. D'Arcangelo G, Nakajima K, Miyata T, Ogawa M, Mikoshiba K, Curran T: **Reelin is a secreted glycoprotein recognized by the CR-50 monoclonal antibody.** *J Neurosci* 1997, **17**(1):23–31.
23. Rogers JT, Rusiana I, Trotter J, Zhao L, Donaldson E, Pak DT, Babus LW, Peters M, Banko JL, Chavis P, Rebeck GW, Hoe HS, Weeber EJ: **Reelin supplementation enhances cognitive ability, synaptic plasticity, and dendritic spine density.** *Learn Mem* 2011, **18**(9):558–564.
24. Ventruti A, Kazdoba TM, Niu S, D'Arcangelo G: **Reelin deficiency causes specific defects in the molecular composition of the synapses in the adult brain.** *Neuroscience* 2011, **189:**32–42.
25. Hellwig S, Hack I, Kowalski J, Brunne B, Jarowyj J, Unger A, Bock HH, Junghans D, Frotscher M: **Role for Reelin in neurotransmitter release.** *J Neurosci* 2011, **31**(7):2352–2360.
26. Matsuki T, Matthews RT, Cooper JA, van der Brug MP, Cookson MR, Hardy JA, Olson EC, Howell BW: **Reelin and stk25 have opposing roles in neuronal polarization and dendritic Golgi deployment.** *Cell* 2010, **143**(5):826–836.
27. Leemhuis J, Bouche E, Frotscher M, Henle F, Hein L, Herz J, Meyer DK, Pichler M, Roth G, Schwan C, Bock HH: **Reelin signals through apolipoprotein E receptor 2 and Cdc42 to increase growth cone motility and filopodia formation.** *J Neurosci* 2010, **30**(44):14759–14772.
28. Borrell V, Del Rio JA, Alcantara S, Derer M, Martinez A, D'Arcangelo G, Nakajima K, Mikoshiba K, Derer P, Curran T, Soriano E: **Reelin regulates the development and synaptogenesis of the layer-specific entorhino-hippocampal connections.** *J Neurosci* 1999, **19**(4):1345–1358.
29. Borrell V, Pujadas L, Simo S, Dura D, Sole M, Cooper JA, Del Rio JA, Soriano E: **Reelin and mDab1 regulate the development of hippocampal connections.** *Mol Cell Neurosci* 2007, **36**(2):158–173.
30. Wu P, Li MS, Yu DM, Deng JB: **Reelin, a guidance signal for the regeneration of the entorhino-hippocampal path.** *Brain Res* 2008, **1208:**1–7.
31. Su J, Haner CV, Imbery TE, Brooks JM, Morhardt DR, Gorse K, Guido W, Fox MA: **Reelin is required for class-specific retinogeniculate targeting.** *J Neurosci* 2011, **31**(2):575–586.
32. Trommsdorff M, Gotthardt M, Hiesberger T, Shelton J, Stockinger W, Nimpf J, Hammer RE, Richardson JA, Herz J: **Reeler/Disabled-like disruption of neuronal migration in knockout mice lacking the VLDL receptor and ApoE receptor 2.** *Cell* 1999, **97**(6):689–701.
33. Benhayon D, Magdaleno S, Curran T: **Binding of purified Reelin to ApoER2 and VLDLR mediates tyrosine phosphorylation of Disabled-1.** *Brain Res Mol Brain Res* 2003, **112**(1–2):33–45.
34. Howell BW, Hawkes R, Soriano P, Cooper JA: **Neuronal position in the developing brain is regulated by mouse disabled-1.** *Nature* 1997, **389**(6652):733–737.
35. Howell BW, Herrick TM, Hildebrand JD, Zhang Y, Cooper JA: **Dab1 tyrosine phosphorylation sites relay positional signals during mouse brain development.** *Curr Biol* 2000, **10**(15):877–885.

36. Sheldon M, Rice DS, D'Arcangelo G, Yoneshima H, Nakajima K, Mikoshiba K, Howell BW, Cooper JA, Goldowitz D, Curran T: **Scrambler and yotari disrupt the disabled gene and produce a reeler-like phenotype in mice.** *Nature* 1997, **389**(6652):730–733.
37. Land PW, Kyonka E, Shamalla-Hannah L: **Vesicular glutamate transporters in the lateral geniculate nucleus: expression of VGLUT2 by retinal terminals.** *Brain Res* 2004, **996**(2):251–254.
38. Singh R, Su J, Brooks JM, Terauchi A, Umemori H, Fox MA: **Fibroblast Growth Factor 22 contributes to the development of retinal nerve terminals in the dorsal lateral geniculate nucleus.** *Front Mol Neurosci* 2012, **4**:61.
39. Jaubert-Miazza L, Green E, Lo FS, Bui K, Mills J, Guido W: **Structural and functional composition of the developing retinogeniculate pathway in the mouse.** *Vis Neurosci* 2005, **22**(5):661–676.
40. Bickford ME, Slusarczyk A, Dilger EK, Krahe TE, Kucuk C, Guido W: **Synaptic development of the mouse dorsal lateral geniculate nucleus.** *J Comp Neurol* 2010, **518**(5):622–635.
41. Fujiyama F, Hioki H, Tomioka R, Taki K, Tamamaki N, Nomura S, Okamoto K, Kaneko T: **Changes of immunocytochemical localization of vesicular glutamate transporters in the rat visual system after the retinofugal denervation.** *J Comp Neurol* 2003, **465**(2):234–249.
42. Guido W: **Refinement of the retinogeniculate pathway.** *J Physiol* 2008, **586**(Pt 18):4357–4362.
43. Rice DS, Nusinowitz S, Azimi AM, Martinez A, Soriano E, Curran T: **The reelin pathway modulates the structure and function of retinal synaptic circuitry.** *Neuron* 2001, **31**(6):929–941.
44. Trotter JH, Klein M, Jinwal UK, Abisambra JF, Dickey CA, Tharkur J, Masiulis I, Ding J, Locke KG, Rickman CB, Birch DG, Weeber EJ, Herz J: **ApoER2 function in the establishment and maintenance of retinal synaptic connectivity.** *J Neurosci* 2011, **31**(40):14413–14423.
45. Botchkina GI, Morin LP: **Specialized neuronal and glial contributions to development of the hamster lateral geniculate complex and circadian visual system.** *J Neurosci* 1995, **15**(1 Pt 1):190–201.
46. Dulabon L, Olson EC, Taglienti MG, Eisenhuth S, McGrath B, Walsh CA, Kreidberg JA, Anton ES: **Reelin binds alpha3beta1 integrin and inhibits neuronal migration.** *Neuron* 2000, **27**(1):33–44.
47. Schmid RS, Jo R, Shelton S, Kreidberg JA, Anton ES: **Reelin, integrin and DAB1 interactions during embryonic cerebral cortical development.** *Cereb Cortex* 2005, **15**(10):1632–1636.
48. Dong E, Caruncho H, Liu WS, Smalheiser NR, Grayson DR, Costa E, Guidotti A: **A reelin-integrin receptor interaction regulates Arc mRNA translation in synaptoneurosomes.** *Proc Natl Acad Sci USA* 2003, **100**(9):5479–5484.
49. Rodriguez MA, Pesold C, Liu WS, Kriho V, Guidotti A, Pappas GD, Costa E: **Colocalization of integrin receptors and reelin in dendritic spine postsynaptic densities of adult nonhuman primate cortex.** *Proc Natl Acad Sci USA* 2000, **97**(7):3550–3555.
50. Stipp CS, Hemler ME: **Transmembrane-4-superfamily proteins CD151 and CD81 associate with alpha 3 beta 1 integrin, and selectively contribute to alpha 3 beta 1-dependent neurite outgrowth.** *J Cell Sci* 2000, **113**(Pt 11):1871–1882.
51. Ivins JK, Yurchenco PD, Lander AD: **Regulation of neurite outgrowth by integrin activation.** *J Neurosci* 2000, **20**(17):6551–6560.
52. Ivins JK, Colognato H, Kreidberg JA, Yurchenco PD, Lander AD: **Neuronal receptors mediating responses to antibody activated laminin-1.** *J Neurosci* 1998, **18**(23):9703–9715.
53. Young-Pearse TL, Chen AC, Chang R, Marquez C, Selkoe DJ: **Secreted APP regulates the function of full-length APP in neurite outgrowth through interaction with integrin beta1.** *Neural Dev* 2008, **3**:15.
54. Billnitzer AJ, Barskaya I, Yin C, Perez RG: **APP independent and dependent effects on neurite outgrowth are modulated by the receptor associated protein (RAP).** *J Neurochem* 2012, **124**(1):123–132.
55. Caldwell JH, Klevanski M, Saar M, Müller UC: **Roles of the amyloid precursor protein family in the peripheral nervous system.** *Mech Dev* 2012, **29**(12):112–118.
56. Hoe HS, Lee KJ, Carney RS, Lee J, Markova A, Lee JY, Howell BW, Hyman BT, Pak DT, Bu G, Rebeck GW: **Interaction of reelin with amyloid precursor protein promotes neurite outgrowth.** *J Neurosci* 2009, **29**(23):7459–7473.
57. Ho T, Vessey KA, Cappai R, Dinet V, Mascarelli F, Ciccotosto GD, Fletcher EL: **Amyloid precursor protein is required for normal function of the rod and cone pathways in the mouse retina.** *PLoS One* 2012, **7**(1):e29892.
58. Angst BD, Marcozzi C, Magee AI: **The cadherin superfamily: diversity in form and function.** *J Cell Sci* 2001, **114**(Pt 4):629–641.
59. Senzaki K, Ogawa M, Yagi T: **Proteins of the CNR family are multiple receptors for Reelin.** *Cell* 1999, **99**(6):635–647.
60. Jossin Y, Ignatova N, Hiesberger T, Herz J, de Lambert RC, Goffinet AM: **The central fragment of Reelin, generated by proteolytic processing in vivo, is critical to its function during cortical plate development.** *J Neurosci* 2004, **24**(2):514–521.
61. Sanes JR, Zipursky SL: **Design principles of insect and vertebrate visual systems.** *Neuron* 2010, **66**(1):15–36.
62. Zipursky SL, Sanes JR: **Chemoaffinity revisited: dscams, protocadherins, and neural circuit assembly.** *Cell* 2010, **143**(3):343–353.
63. Honjo M, Tanihara H, Suzuki S, Tanaka T, Honda Y, Takeichi M: **Differential expression of cadherin adhesion receptors in neural retina of the postnatal mouse.** *Invest Ophthalmol Vis Sci* 2000, **41**(2):546–551.
64. Lefebvre JL, Zhang Y, Meister M, Wang X, Sanes JR: **gamma-Protocadherins regulate neuronal survival but are dispensable for circuit formation in retina.** *Development* 2008, **135**(24):4141–4151.
65. Lefebvre JL, Kostadinov D, Chen WV, Maniatis T, Sanes JR: **Protocadherins mediate dendritic self-avoidance in the mammalian nervous system.** *Nature* 2012, **488**(7412):517–521.
66. Osterhout JA, Josten N, Yamada J, Pan F, Wu SW, Nguyen PL, Panagiotakos G, Inoue YU, Egusa SF, Volgyi B, Inoue T, Bloomfield SA, Barres BA, Berson DM, Feldheim DA, Huberman AD: **Cadherin-6 mediates axon-target matching in a non-image-forming visual circuit.** *Neuron* 2011, **71**(4):632–639.
67. Hui DY, Basford JE: **Distinct signaling mechanisms for apoE inhibition of cell migration and proliferation.** *Neurobiol Aging* 2005, **26**(3):317–323.
68. Blake SM, Strasser V, Andrade N, Duit S, Hofbauer R, Schneider WJ, Nimpf J: **Thrombospondin-1 binds to ApoER2 and VLDL receptor and functions in postnatal neuronal migration.** *EMBO J* 2008, **27**(22):3069–3080.
69. Oganesian A, Armstrong LC, Migliorini MM, Strickland DK, Bornstein P: **Thrombospondins use the VLDL receptor and a nonapoptotic pathway to inhibit cell division in microvascular endothelial cells.** *Mol Biol Cell* 2008, **19**(2):563–571.
70. Volgyi B, Chheda S, Bloomfield SA: **Tracer coupling patterns of the ganglion cell subtypes in the mouse retina.** *J Comp Neurol* 2009, **512**(5):664–687.
71. Coombs J, van der List D, Wang GY, Chalupa LM: **Morphological properties of mouse retinal ganglion cells.** *Neuroscience* 2006, **140**(1):123–136.
72. Kong JH, Fish DR, Rockhill RL, Masland RH: **Diversity of ganglion cells in the mouse retina: unsupervised morphological classification and its limits.** *J Comp Neurol* 2005, **489**(3):293–310.
73. Sun W, Li N, He S: **Large-scale morphological survey of mouse retinal ganglion cells.** *J Comp Neurol* 2002, **451**(2):115–126.
74. Su J, Gorse K, Ramirez F, Fox MA: **Collagen XIX is expressed by interneurons and contributes to the formation of hippocampal synapses.** *J Comp Neurol* 2010, **518**(2):229–253.
75. Yamamoto T, Sakakibara S, Mikoshiba K, Terashima T: **Ectopic corticospinal tract and corticothalamic tract neurons in the cerebral cortex of yotari and reeler mice.** *J Comp Neurol* 2003, **461**(1):61–75.
76. Su J, Stenbjorn RS, Gorse K, Su K, Hauser KF, Ricard-Blum S, Pihlajaniemi T, Fox MA: **Target-derived matricryptins organize cerebellar synapse formation through alpha3beta1 integrins.** *Cell Rep* 2012, **2**(2):223–230.

doi:10.1186/1749-8104-8-11
**Cite this article as:** Su *et al.*: Contributions of VLDLR and LRP8 in the establishment of retinogeniculate projections. *Neural Development* 2013 **8**:11.